Shape coexistence in ^{178}Hg

C. Müller-Gatermann,[1,*] A. Dewald,[1] C. Fransen,[1] K. Auranen,[2,†] H. Badran,[2] M. Beckers,[1] A. Blazhev,[1] T. Braunroth,[1] D. M. Cullen,[3] G. Fruet,[4] A. Goldkuhle,[1] T. Grahn,[2] P. T. Greenlees,[2] A. Herzáň,[5,6,2] U. Jakobsson,[7,2] D. Jenkins,[8] J. Jolie,[1] R. Julin,[2] S. Juutinen,[2] J. Konki,[2,‡] M. Leino,[2] J. Litzinger,[1] K. Nomura,[9] J. Pakarinen,[2] P. Peura,[10,2] M. G. Procter,[3] P. Rahkila,[2] P. Ruotsalainen,[11,2] M. Sandzelius,[2] J. Sarén,[2] C. Scholey,[2] J. Sorri,[12,2] S. Stolze,[2,†] M. J. Taylor,[13,3] J. Uusitalo,[2] and K. O. Zell[1]

[1]*Institut für Kernphysik der Universität zu Köln, Zülpicher Straße 77, D-50937 Köln, Germany*
[2]*University of Jyvaskyla, Department of Physics, P.O. Box 35, FI-40014 Jyvaskyla, Finland*
[3]*Schuster Laboratory, University of Manchester, Manchester M13 9PL, United Kingdom*
[4]*Université de Strasbourg, CNRS, IPHC UMR 7178, F-67000 Strasbourg, France*
[5]*Institute of Physics, Slovak Academy of Sciences, SK-84511 Bratislava, Slovakia*
[6]*Oliver Lodge Laboratory, University of Liverpool, Liverpool L69 7ZE, United Kingdom*
[7]*Laboratory of Radiochemistry, Department of Chemistry, P.O. Box 55, FI-00014 University of Helsinki, Finland*
[8]*Department of Physics, University of York, YO10 5DD York, United Kingdom*
[9]*Advanced Science Research Center, Japan Atomic Energy Agency, Tokai, 319-1195 Ibaraki, Japan*
[10]*Helsinki Institute of Physics, University of Helsinki, P.O. Box 64, 00014 Helsinki, Finland*
[11]*TRIUMF, Westbrook Mall, Vancouver, British Columbia V6T 2A3, Canada*
[12]*Sodankylä Geophysical Observatory, University of Oulu, FI-99600 Sodankylä, Finland*
[13]*Division of Cancer Sciences, University of Manchester, Manchester M13 9PL, United Kingdom*

(Received 5 February 2019; published 21 May 2019)

Lifetime measurements of excited states in ^{178}Hg have been performed using the ^{103}Rh(^{78}Kr, $p2n$) reaction at a beam energy of 354 MeV. The recoil-decay tagging (RDT) technique was applied to select the ^{178}Hg nuclei and associate the prompt γ rays with the correlated characteristic ground-state α decay. Lifetimes of the four lowest yrast states of ^{178}Hg have been determined using the recoil distance Doppler-shift (RDDS) method. The experimental data are compared to theoretical predictions with focus on shape coexistence. The results confirm the shift of the deformed prolate structures to higher lying states but also indicate their increasing deformation with decreasing neutron number.

DOI: 10.1103/PhysRevC.99.054325

I. INTRODUCTION

Even-even nuclei close to shell closures have been the subject of numerous experimental and theoretical studies [1,2]. Phenomena like shape coexistence [2] and shape transitions [3] have been observed around the shell closure at $Z = 82$ near the neutron $N = 104$ midshell. The shapes of the neutron-deficient even-even Hg isotopes [4–6] are interpreted to be determined by the excitation of protons across the $Z = 82$ shell closure, forming "intruder states." The intruder states may have a significant prolate deformation [7] coexisting with less deformed oblate ground states. The level-energy systematics show a rather constant trend for the band build upon the weak oblate minimum, while a prolate deformed intruder band exhibiting a parabolic trend with respect to the neutron number shows a minimum at ^{182}Hg. The intruding band crosses the yrast line at ^{188}Hg and around ^{176}Hg, suggesting together with the known experimental data that the interpretation holds for all midshell Hg nuclei (Fig. 1). Nevertheless, the composition of the wave function of the 2_1^+ states changes dramatically with respect to the neutron number [5,6]. The prolate band build upon an excited 0^+ state can be related to similar structures in the neighboring Pb nuclei. An overview of the spectroscopic studies in this mass region ranging from $_{80}$Hg to $_{84}$Po isotopes is given in Ref. [8]. In the odd-mass nuclei ^{183,185}Hg, a dramatic change in charge radius (compared to the neighboring even-mass Hg nuclei) was discovered in 1972 with isotope shift measurements [9]. Recently, the available data were extended to ^{177}Hg and the microscopic origin of the shape staggering effect was explained with the aid of the Monte Carlo shell model (MCSM) [10]. These larger charge radii are not observed in the more neutron-deficient isotopes with masses below 181. To date, the most neutron-deficient isotope of mercury for which transition probabilities are known is ^{180}Hg. The even-mass neighbor ^{178}Hg is predicted to be the start point of a shape transition by several theoretical models such as total Routhian surface (TRS) calculations [11], mean-field approaches, and the interacting boson model

*cmgater@ikp.uni-koeln.de
†Present address: Physics Division, Argonne National Laboratory, Argonne, Illinois 60439, USA.
‡Present address: CERN, CH-1211 Geneva 23, Switzerland.

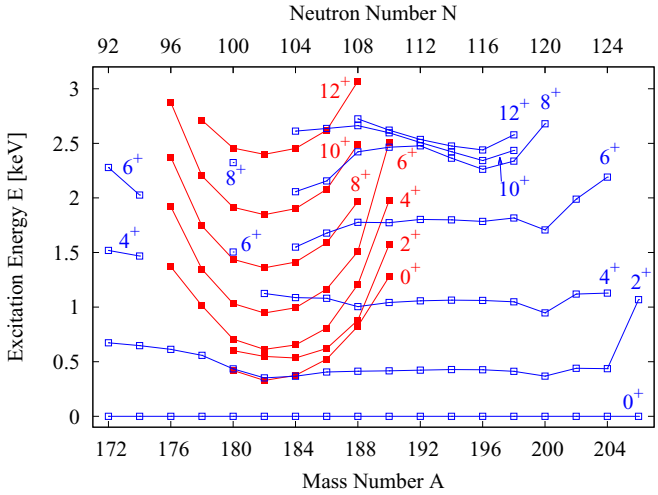

FIG. 1. Level energy systematics of the even-mass mercury isotopes. Red filled squares refer to the assumed intruder states while blue open squares refer to the assumed oblate states. The figure is adopted from Ref. [6].

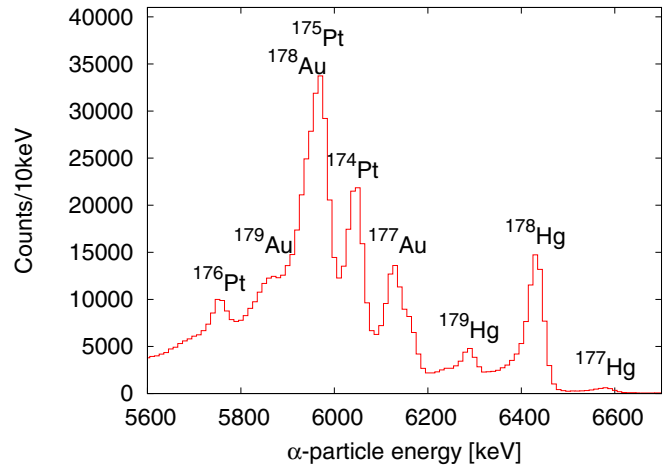

FIG. 2. Spectrum of observed α-particle energies occurring within 2000 ms of an ion being implanted into the same DSSSD pixel. Assignments for the peaks are indicated. See text for details.

(IBM) with configuration mixing [12]. Therefore, to address the question of shape evolution toward even more neutron-deficient Hg isotopes, lifetime measurements of excited states in ^{178}Hg have been performed in the present work.

II. EXPERIMENTAL DETAILS

Excited states of ^{178}Hg were populated in a heavy-ion induced fusion-evaporation reaction at the Accelerator Laboratory of the University of Jyväskylä, where lifetimes of excited states were measured with the Differential Plunger for Unbound Nuclear States (DPUNS) [13]. The reaction ^{103}Rh(^{78}Kr, $p2n$)^{178}Hg with a beam energy of 354 MeV provided an initial recoil velocity of $v/c = 3.9\%$, with a target thickness of 1 mg/cm^2. The typical beam current was of the order of 3–5 pnA, limited by heating of the stretched plunger target and degrader foils and the maximum counting rate of 30 kHz per JUROGAM II HPGe detector. The JUROGAM II Ge-detector array consisted of 24 EUROGAM (European Gamma-ray Microscope) Clover detectors [14] in two rings at 75.5° and 104.5° and two rings with tapered EUROGAM phase I [15] or GASP (Gamma-ray Spectrometer) type [16] germanium detectors at 133.6° (10 detectors) and 157.6° (5 detectors) with respect to the beam direction. All detectors were Compton-suppressed. The DPUNS was installed at the JUROGAM II target position to perform recoil distance Doppler-shift (RDDS) lifetime measurements of excited states in ^{178}Hg. A 1.6 mg/cm^2 Mg degrader foil reduced the energy of the fusion products and allowed them to recoil into the Recoil Ion Transport Unit (RITU) [17,18] with a velocity of $v/c = 2.3\%$. RITU was filled with helium gas at a pressure of 0.6 mbar and separated the evaporation residues from the fission background and scattered beam according to their magnetic rigidity. The gas of RITU cooled the target and degrader foils, allowing the aforementioned relatively high beam intensities to be used. The recoils were transported through RITU to the Gamma Recoil Electron Alpha Tagging (GREAT) spectrometer [19] at the focal plane. The recoils passed through a multiwire proportional counter (MWPC) and were implanted into a pair of double-sided silicon strip detectors (DSSSDs). Discrimination between evaporation residues and scattered beam particles was achieved on the basis of energy loss in the MWPC and the time of flight between the MWPC and DSSSDs. With an anticoincidence between the MWPC and the DSSSDs, the decays in the DSSSD are distinguishable from the implantation events. For the identification of the evaporation residues, the recoil-decay tagging (RDT) technique [20] was applied, whereby an α decay is correlated with a previously implanted recoil within a specific search time. The γ rays associated with the recoil can then be extracted. To remove the random coincidences in the γ-ray spectra, stemming mainly from Coulomb excitation of the beam, the time difference spectrum between the JUROGAM II Ge detectors signals and the MWPC signal was used. The events of the pure prompt peak were selected by subtracting events of the plateau outside of the prompt peak with background using the same window sizes. For the tagging of ^{178}Hg, a search time of 2000 ms, which is about seven times the half-life, between an implantation and an α-decay event at the same position in the DSSSDs was set together with a gate on the ground state α-decay energy of 6.43 MeV and a width of 160 keV. To increase the level of statistics, recoil-α-α correlations to the daughter nucleus ^{174}Pt were also employed. If the α particle emitted by ^{178}Hg escapes, the correlated chain can still be recovered by respective cuts on time and energy. When taking this effect into account, the statistics are increased by 25%, which is expected from the geometrical escape probability and the α-decay branch of ^{174}Pt. No contamination with ^{174}Pt events is seen in the γ-ray spectra, as an earlier decay event within the time window for ^{178}Hg is required. All detector signals were passed to the triggerless Total Data Readout (TDR) data acquisition system [21]. The data were analyzed using the GRAIN [22] and TV [23] software packages. A spectrum of observed α-particle energies is presented in Fig. 2 showing the statistics for 60 h, which corresponds to

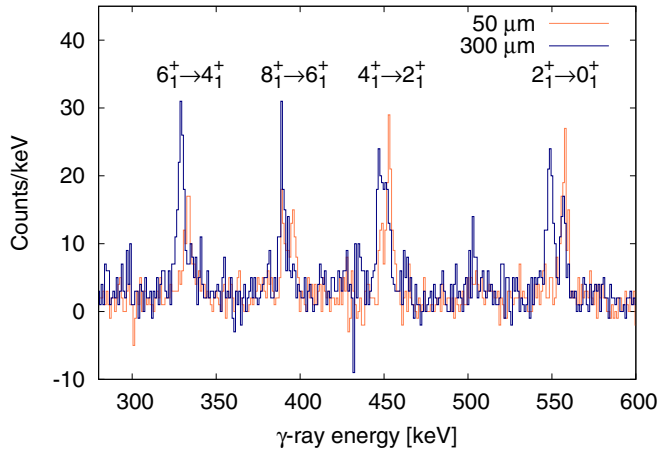

FIG. 3. Background subtracted γ-ray energy spectra measured with the JUROGAM II detectors in the ring at 157.6° (five detectors) for the shortest and longest distances. Assignments for the lowest four yrast transitions are indicated. See text for details.

one target-to-degrader distance. The region of interest around ^{178}Hg shows no contaminations. Only the decays of ^{178}Au and ^{175}Pt are not separated and in the case of ^{177}Au the peak is broader due to the decay of an excited isomeric state. In Fig. 3, the resulting γ-ray spectra for the transitions of interest are shown for the shortest and longest distances when the procedures to select ^{178}Hg described above are used. The background is low with little contamination. Only the outermost ring at 157.6° could be used to extract lifetimes due to the low Doppler shifts and an energy resolution of around 3 keV for the unshifted component (after Doppler correction). The γ-ray spectra of the Clover detectors (around 90°), having most of the efficiency and showing almost no Doppler shift, were summed up over all plunger distances and were used to determine the initial population of the individual states. In total, four different relative target-to-degrader distances were measured and analyzed, namely 50, 100, 200, and 300 µm.

III. LIFETIME ANALYSIS

Because of the very limited number of distances and the fact that only γ-ray singles spectra could be analyzed, where delayed feeding from higher states is relevant, the differential decay curve method (DDCM) [24] was not applied. The lifetime of an excited state can be determined from the decay curve, which is the intensity ratio of the degraded I_D and the sum of fast I_T and degraded peaks of γ rays depopulating the level of interest as a function of the distance d between the foils, $R(d) = I_D(d)/[I_D(d) + I_T(d)]$ [25]. In the case of a γ-ray singles analysis, all observed feeding transitions have to be taken into account. The solution of the corresponding system of differential equations (Bateman equations) is fitted to the decay curve. For such an analysis, exact absolute distance information is crucial, especially when so few target-to-degrader distances were used. The plunger device used provides relative distance information with a precision of ≈ 0.1 µm, but always with an offset caused by an unknown zero point which depends on the quality of the target and degrader

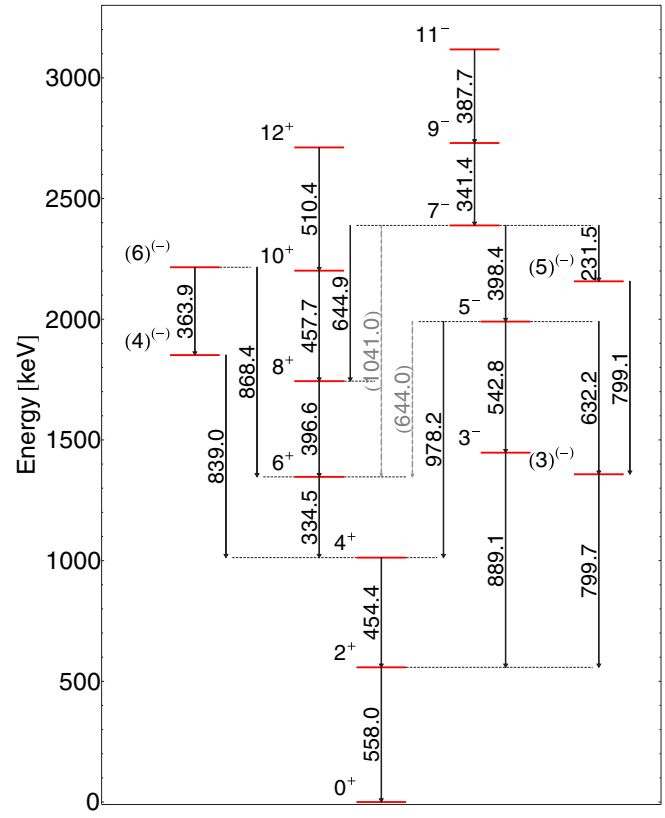

FIG. 4. Partial level scheme of ^{178}Hg up to the 11_1^- state, which is the highest lying state taken into account for feeding. γ energies, spins, and parity are taken from Ref. [27]. See text for details.

surface. An offset of 19(1) µm was determined by measuring the capacitance of the target-degrader system, as described in Refs. [25,26]. This translates to absolute time of flights between the target and the degrader of 5.52, 9.80, 18.04, and 26.27 ps for the relative target-to-degrader distances of 50, 100, 200, and 300 µm, respectively.

The effect of unobserved feeding transitions to the level of interest must be taken into account in the analysis of singles RDDS data. Therefore, the total statistics of all Clover detectors around 90° was added up for all distances. With these spectra, the efficiency-corrected initial populations were fixed for all known states up to the 11_1^- state and are in agreement with those of Ref. [27]. The efficiencies of the JUROGAM II Ge detectors were determined using a ^{152}Eu source. A partial level scheme up to the highest lying state observed in this work and taken into account in the feeding analysis is shown in Fig. 4.

The effective lifetimes of the feeding transitions were then fitted together with the state of interest, beginning with the highest lying state (8_1^+ state) for which a lifetime determination is possible. All lifetimes were then fixed and used in the following analysis of lower lying states. The uncertainty of the lifetime of the feeding transition was taken into account in the error of the decaying transition. A common assumption, that all unobserved feeding has the same time behavior as the observed feeding, i.e., the feeder with the highest intensity, was wrong in this case. Significantly longer feeding time was

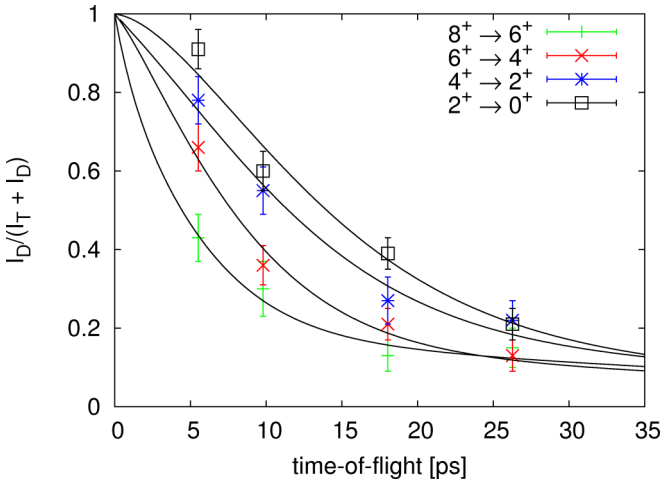

FIG. 5. Decay curves for the ground-state band up to the 8_1^+ state in ^{178}Hg constructed from the RDT singles γ-ray spectra recorded with five JUROGAM II detectors at 157.6°. The smooth lines correspond to the best fits.

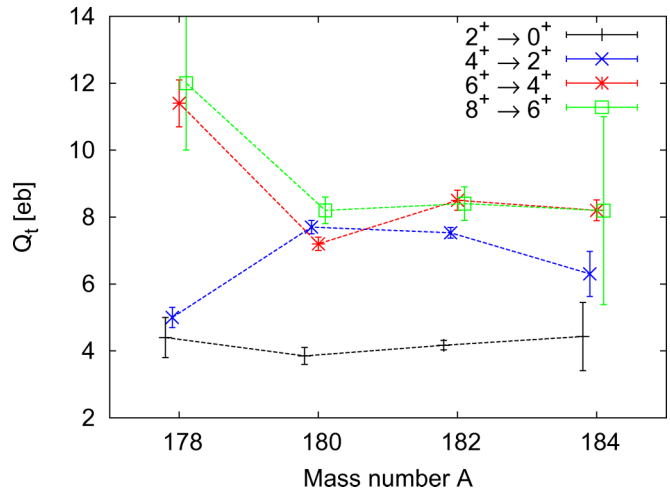

FIG. 6. Absolute values of transition quadrupole moments for the neutron-deficient Hg isotopes near midshell. See text for details.

needed to reproduce the decay curves. This is ascribed to strongly populated negative-parity states, e.g., the 7_1^- state, which branch out significantly and have to be taken into account for each state with different cascades. The decay curves for the yrast states are presented in Fig. 5 and show good agreement with the experimental data. Since the feeding assumptions affect all states of interest and are based on experimentally determined initial populations and branching ratios, they seem plausible. The experimental lifetime data stems from normalized fits of the spectra in the outermost ring with fixed peak widths and positions. The Doppler shift of γ rays in the spectra from the ring of detectors at 133° was not large enough to allow an independent analysis, but they were checked for consistency.

The results of the lifetime analysis are summarized in Table I. By using the rotational model with the assumption of a rotating quadrupole deformed nucleus, the absolute values of transition quadrupole moments Q_t and deformation parameters β_2 are given in the same table together with the corresponding $B(E2)$ values. For the determination of deformation parameters,

$$\beta_2 = 0.625(-5a + \sqrt{25a^2 + 16aQ_t})/a,$$
$$a = \frac{3}{\sqrt{5\pi}ZR_0^2}, \quad (1)$$

was used, where Z is the atomic number and R_0 is the nuclear radius.

TABLE I. Electromagnetic properties of the lowest yrast states in ^{178}Hg.

I^π [27]	E_γ [keV] [27]	τ [ps]	$B(E2)$ [W.u.]	$\lvert Q_t\rvert$ [eb]	$\lvert\beta_2\rvert$
2_1^+	558.0	3.8(9)	$66(^{+20}_{-12})$	$4.4(^{+6}_{-5})$	$0.16(^{+2}_{-2})$
4_1^+	454.4	5.7(6)	$120(^{+14}_{-11})$	$5.0(^{+3}_{-2})$	$0.18(^{+1}_{-1})$
6_1^+	334.5	4.4(5)	$690(^{+90}_{-70})$	$11.4(^{+7}_{-6})$	$0.41(^{+3}_{-2})$
8_1^+	396.6	1.7(5)	$800(^{+300}_{-200})$	$11.9(^{+20}_{-14})$	$0.43(^{+8}_{-5})$

IV. DISCUSSION

The $B(E2)$ values shown in Table I indicate a structural change for the lowest lying states. This is known for Hg isotopes with $A \gtrsim 180$ at the 2_1^+ state [4]. The Q_t values for $^{178-184}$Hg as a function of mass number A are shown in Fig. 6. The weakly deformed oblate configuration, which forms also the ground-state mixes with the prolate deformed structure of the intruder states. The 2_1^+ state for $A \geqslant 180$ is already strongly mixed and reduces the transition probability of the $2_1^+ \to 0_1^+$ transition. Mixing calculations for these midshell nuclei which were performed in Refs. [5] and [6] as well as Ref. [4] for ^{182}Hg reveal up to $\approx 80\%$ prolate contribution to the wave function of the 2_1^+ state. At higher spins, the Q_t values stay rather constant and a deformation of $\beta_2 \approx 0.25$ can be attributed to the rotational structure corresponding to the prolate band. The authors of Ref. [5] assume from Coulomb-excitation measurements and the two-level mixing calculations of Ref. [6] that there significant changes in the composition of the 2_1^+ states. To reproduce the $B(E2)$ values in ^{178}Hg, a two-band mixing calculation assuming interband transitions to be forbidden has been performed. The calculation suggests that the 2_1^+ state has an $\approx 80\%$ contribution of oblate deformed structure in the wave function similar to the ground state. The 4_1^+ state wave function changes to an $\approx 80\%$ portion of the prolate band and reduces the $4_1^+ \to 2_1^+$ transition strength. For the higher lying states, an unperturbed rotational band can be assumed with a deformation of $\beta_2 \approx 0.4$ due to the large Q_t values for the respective transitions. Since the ground state and the 2_1^+ state have a large overlap of the wave functions, one could extract a deformation of $\beta \approx 0.15$, which is consistent with the ground-state deformations of heavier Hg isotopes extracted from isotope shift measurements. It is not meaningful to deduce a deformation from the transition between the structures because the small overlap of the wave functions lowers the transition strength.

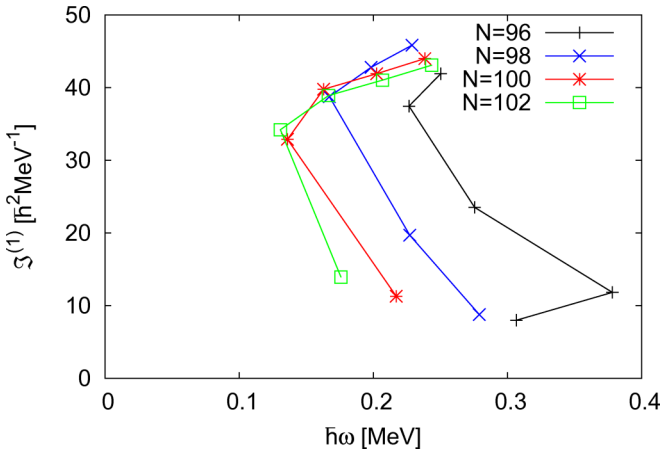

FIG. 7. Kinetic moments of inertia $\Im^{(1)}(J)$ for the Hg isotopes as a function of frequency $\omega(J \to J-2)$ for transitions along the yrast line up to the 10^+ state. The figure is adopted from Ref. [31]. See text for details.

The shape change seems to be shifted toward the 4_1^+ state, consistent with the trend seen by Bree *et al.* [5]. A larger deformation of $\beta_2 \approx 0.4$ is revealed (extracted from the pure 6_1^+, 8_1^+ states). This so-called intermediate deformation [between normal and superdeformation (SD)] is discussed in Ref. [28] and is explained by the shape-driving effect of intruder neutron orbitals. These are clearly manifested by the negative-parity band built upon a 11^- state in ^{186}Hg (band 3 in Ref. [28]) and the population of a pair of quasineutrons to configurations with involvement of the $\nu[651]\frac{1}{2}$ orbital. The occupation of these orbitals is also expected for the SD configurations of heavier Hg isotopes [29]. SD bands leading to various shape-coexisting configurations in the light Hg isotopes with $N \leqslant 98$ were predicted in Ref. [30]. The deformation is also consistent with predictions of TRS calculations presented in Ref. [11], in which the authors state that for the nuclei ^{172,174,176}Hg the near-oblate ground state evolves steadily toward a more spherical shape with decreasing N as the $N = 82$ closed shell is approached. Second, no prolate minimum is seen in the TRS calculations with $\beta_2 \approx 0.25$ for $^{172-176}$Hg, but for increasing neutron number a well-deformed minimum ($\beta_2 \approx 0.35$) starts to develop and is first observed in ^{176}Hg. The level energy systematics showing the prolate (red filled squares) as well as the oblate (blue open squares) structures are tracked throughout the Hg isotopes and depicted in Fig. 1. For the more neutron-deficient isotope ^{178}Hg, the energy of the prolate structure increases and the mixing with low-lying states decreases as described above. The structural change becomes apparent also in the kinetic moments of inertia $\Im^{(1)}$ along the yrast band. Resuming the statements of Ref. [31], there are well-established generic properties of the moments of inertia such as their increase with deformation, or that for the same value of $|\beta_2|$ the moment of inertia is larger for prolate deformations than for oblate ones. In Fig. 7, the kinetic moments of inertia are shown for the yrast bands in $^{176-182}$Hg as a function of frequency $\omega(J \to J-2)$. The first observation is that the moments of inertia for high-spin group at high absolute values can be attributed to a stable deformation (constant moment of inertia for an idealized static rotor). The moment of inertia for $J = 2$ is significantly different from those corresponding to transitions from higher spins. This is consistent with the picture discussed earlier. Second, at $N = 98$ the moment of inertia is lowered for $J = 4$ in comparison to the heavier isotopes, and this trend is continued for $N = 96$ in this case and also for $J = 6$. Confirming the expectation from the level-energy systematics, the influence of an intruding structure is displaced to higher spins. In summary, there is a good agreement between the interpretations deduced from level energies and lifetimes.

Alternative calculations from Ref. [12] are based on Hartree-Fock-Bogoliubov (HFB) methodology using the Gogny-D1M energy density functional (EDF), which is mapped on the corresponding energy surface of the IBM with configuration mixing. In this case, the proton-neutron IBM (IBM-2) is used. For the configuration mixing, only 2p-2h proton excitations were allowed for $^{176-190}$Hg. This results in a near-spherical structure for ^{172}Hg with a slight prolate minimum evolving toward ^{176}Hg of $\beta_2 \approx 0.25$–0.3. For the heavier Hg isotopes, this minimum gets more pronounced but does not change its quadrupole deformation. This description is consistent with the experimental data for $A \geqslant 180$, and unfortunately it cannot reproduce the transition strengths given in Table I. The discrepancy is probably due to the limited model space of the configuration-mixing IBM-2 used in Ref. [12], which comprised only up to 2p-2h proton excitations, as well as the possibility that the mixing between different configurations may not have been properly accounted for in that calculation. In addition, the topology of the potential energy surface is rather sensitive to the choice of the underlying EDF. The inclusion of neutron intruder excitations, in the configuration-mixing IBM-2 framework could improve the description of the $B(E2)$ transition rates for the considered Hg nuclei.

Recently, more evidence was given supporting the importance of neutron occupation in Ref. [10]. The authors extended the experimental data on charge radii of the ground state with isotope shift measurements down to ^{177}Hg. The first observation is that the shape staggering of the odd-mass Hg nuclei with respect to their even-mass neighbor breaks down at ^{180}Hg. This means that ^{179}Hg has a near-spherical ground state, whereas the ground state of ^{181}Hg was associated with $\beta_2 = 0.313$. Second, the authors present a Monte Carlo shell model (MCSM) calculation and explain the large deformation for Hg isotopes with $A > 180$ with the strong occupation of specific proton and neutron orbitals, namely the $\pi(h_{\frac{9}{2}})$ and the $\nu(i_{\frac{13}{2}})$ orbitals. This is another hint that the deformation-driving structures move away from the ground state in ^{178}Hg and that the neutron contribution should be also taken into account. The extension of the MCSM calculation to excited states would also be an alternative starting point for interpretations of the data.

The level spacings in ^{176}Hg reveal a change in deformation shifted to the 6_1^+ state [32], continuing the trend seen in the data of this work. $B(E2)$ values of excited states in ^{176}Hg are not known so far. These would test the predictions of the TRS

calculations, especially the evolving prolate minimum with intermediate deformation. However, also independent IBM-2 calculations with configuration mixing allowing specific neutron excitations should be done now systematically with the new data available.

V. SUMMARY AND CONCLUSIONS

Excited states in the neutron-deficient nucleus ^{178}Hg were populated in heavy-ion fusion-evaporation reactions and studied using the JUROGAM II and GREAT spectrometers, coupled to the DPUNS and the gas-filled separator RITU. The RDT technique was applied to identify the ^{178}Hg nuclei and the RDDS method was used to determine lifetimes of yrast states up to the 8_1^+ state for the first time. Deformation parameters β_2 were extracted from the corresponding $B(E2)$ values. The 2_1^+ state shows a deformation comparable to the ground state and the ground states in the heavier neighboring even-even Hg isotopes. It is expected from energy systematics that the deformation-driving structures shift toward higher excitation energies. This is verified by experimental transition strengths and a mixing calculation. For the higher lying states, an intermediate deformation between normal and superdeformation has been attributed, which is a new phenomenon in the chain of the Hg isotopes. Consistency with TRS calculations and isotope shift measurements propose ^{178}Hg to be at the point where the nuclear structure changes. This can also be seen from the 2^+ state energies in Fig. 1. It is proposed to include also specific neutron intruder excitations for systematic IBM-2 calculations including the new data. An alternative approach would be to extend the MCSM calculations to excited states. From an experimental point of view, $B(E2)$ values of excited states in the even-even neighbor ^{176}Hg would be very interesting for comparison. Using the largest available Ge-detector arrays in combination with large acceptance gas-filled recoil separators, this goal seems feasible although on the edge of the detection limit.

ACKNOWLEDGMENTS

This work was supported by the Deutsche Forschungs Gemeinschaft (DFG) under Contract No. DE 1516/3-1, by the EU Seventh Framework Programme, "Integrating Activities—Transnational Access" Project No. 262010 (ENSAR), by the Academy of Finland under the Finnish Centre of Excellence Programme (Nuclear and Accelerator Based Physics Programme at JYFL), by the Slovak Research and Development Agency under Contract No. APVV-15-0255, and by the Slovak grant agency VEGA under Contract No. 2/0129/17. The authors acknowledge the support of GAMMAPOOL for the loan of the JUROGAM II detectors.

[1] T. Grahn, A. Dewald, O. Möller, R. Julin, C. W. Beausang, S. Christen, I. G. Darby, S. Eeckhaudt, P. T. Greenlees, A. Görgen *et al.*, Nucl. Phys. A **801**, 83 (2008).
[2] K. Heyde and J. L. Wood, Rev. Mod. Phys. **83**, 1467 (2011).
[3] P. Cejnar, J. Jolie, and R. F. Casten, Rev. Mod. Phys. **82**, 2155 (2010).
[4] T. Grahn, A. Petts, M. Scheck, P. A. Butler, A. Dewald, M. B. Gomez Hornillos, P. T. Greenlees, A. Görgen, K. Helariutta, J. Jolie *et al.*, Phys. Rev. C **80**, 014324 (2009).
[5] N. Bree, K. Wrzosek-Lipska, A. Petts, A. Andreyev, B. Bastin, M. Bender, A. Blazhev, B. Bruyneel, P. Butler, J. Butterworth *et al.*, Phys. Rev. Lett. **112**, 162701 (2014).
[6] L. P. Gaffney, M. Hackstein, R. D. Page, T. Grahn, M. Scheck, P. A. Butler, P. F. Bertone, N. Bree, R. J. Carroll, M. P. Carpenter *et al.*, Phys. Rev. C **89**, 024307 (2014).
[7] J. E. García-Ramos and K. Heyde, Phys. Rev. C **89**, 014306 (2014).
[8] R. Julin, T. Grahn, J. Pakarinen, and P. Rahkila, J. Phys. G: Nucl. Part. Phys. **43**, 024004 (2016).
[9] J. Bonn, G. Huber, H.-J. Kluge, L. Kugler, and E. Otten, Phys. Lett. B **38**, 308 (1972).
[10] B. Marsh, T. Day Goodacre, S. Sels, Y. Tsunoda, B. Andel, A. Andreyev, N. Althubiti, D. Atanasov, A. Barzakh, J. Billowes *et al.*, Nat. Phys. **14**, 1163 (2018).
[11] M. Sandzelius, E. Ganioğlu, B. Cederwall, B. Hadinia, K. Andgren, T. Bäck, T. Grahn, P. Greenlees, U. Jakobsson, A. Johnson *et al.*, Phys. Rev C **79**, 064315 (2009).
[12] K. Nomura, R. Rodríguez-Guzmán, and L. M. Robledo, Phys. Rev. C **87**, 064313 (2013).
[13] M. J. Taylor, D. M. Cullen, A. J. Smith, A. McFarlane, V. Twist, G. A. Alharshan, M. G. Procter, T. Braunroth, A. Dewald, E. Ellinger *et al.*, Nucl. Instr. Meth. A **707**, 143 (2013).
[14] G. Duchêne, F. A. Beck, P. J. Twin, G. de France, D. Curien, L. Han, C. W. Beausang, M. A. Bentley, P. J. Nolan, and J. Simpson, Nucl. Instr. Meth. A **432**, 90 (1999).
[15] C. W. Beausang, S. A. Forbes, P. Fallon, P. J. Nolan, P. J. Twin, J. N. Mo, J. C. Lisle, M. A. Bentley, J. Simpson, F. A. Beck, D. Curien, G. de France, G. Duchêne, and D. Popescu, Nucl. Instr. Meth. A **313**, 37 (1992).
[16] C. R. Alvarez, Nucl. Phys. News **3**, 10 (1993).
[17] M. Leino, J. Äystö, T. Enqvist, P. Heikkinen, A. Jokinen, M. Nurmia, A. Ostrowski, W. H. Trzaska, J. Uusitalo, K. Eskola, P. Armbruster, and V. Ninov, Nucl. Instr. Meth. B **99**, 653 (1995).
[18] J. Sarén, J. Uusitalo, M. Leino, and J. Sorri, Nucl. Instr. Meth. A **654**, 508 (2011).
[19] R. D. Page, A. N. Andreyev, D. E. Appelbe, P. A. Butler, S. J. Freeman, P. T. Greenlees, R.-D. Herzberg, D. G. Jenkins, G. D. Jones, P. Jones *et al.*, Nucl. Instr. Meth. B **204**, 634 (2003).
[20] E. S. Paul, P. J. Woods, T. Davinson, R. D. Page, P. J. Sellin, C. W. Beausang, R. M. Clark, R. A. Cunningham, S. A. Forbes, D. B. Fossan *et al.*, Phys. Rev. C **51**, 78 (1995).
[21] I. Lazarus, E. Appelbe, P. Butler, P. Coleman-Smith, J. Cresswell, S. Freeman, R. Herzberg, I. Hibbert, D. Joss, S. Letts *et al.*, IEEE Trans. on Nucl. Sci. **48**, 567 (2001).
[22] P. Rahkila, Nucl. Instr. Meth. A **595**, 637 (2008).

[23] J. Theuerkauf, S. Esser, S. Krink, M. Luig, N. Nicolay, O. Stuch, and H. Wolters, Program TV, Institute for Nuclear Physics, Cologne, Germany.
[24] A. Dewald, S. Harissopulos, and P. von Brentano, Z. Phys. A **334**, 163 (1989).
[25] T. Alexander and A. Bell, Nucl. Instr. Meth. **81**, 22 (1970).
[26] A. Dewald, O. Möller, and P. Petkov, Prog. Part. Nucl. Phys. **67**, 786 (2012).
[27] E. Achterberg, O. Capurro, and G. Marti, Nuclear Data Sheets **110**, 1473 (2009).
[28] W. C. Ma, J. H. Hamilton, A. V. Ramayya, L. Chaturvedi, J. K. Deng, W. B. Gao, Y. R. Jiang, J. Kormicki, X. W. Zhao, N. R. Johnson *et al.*, Phys. Rev. C **47**, R5(R) (1993).
[29] R. Janssens and T. Khoo, Annu. Rev. Nucl. Part. Sci. **41**, 321 (1991).
[30] W. Nazarewicz, Phys. Lett. B **305**, 195 (1993).
[31] J. M. Yao, M. Bender, and P.-H. Heenen, Phys. Rev. C **87**, 034322 (2013).
[32] M. Muikku, J. F. C. Cocks, K. Helariutta, P. Jones, R. Julin, S. Juutinen, H. Kankaanpää, H. Kettunen, P. Kuusiniemi, M. Leino *et al.*, Phys. Rev. C **58**, R3033(R) (1998).